12.6 A CMOS Molecular Electronics Chip for Single-Molecule Biosensing

Drew A. Hall[1], Nagaraj Ananthapadmanabhan[2], Chulmin Choi[2], Le Zheng[2], Paul P. Pan[2], Carl W. Fuller[2], Pius P. Padayatti[2], Calvin Gardner[2], Daniel Gebhardt[2], Zsolt Majzik[2], Prem Sinha[2], Paul W. Mola[2], Barry Merriman[2]

[1]University of California, San Diego, CA
[2]Roswell Biotechnology, San Diego, CA

Molecular electronics is the concept of integrating single molecules into circuits as functional elements. For nearly 50 years, this has been envisioned as a way to extend Moore's Law to physical scaling limits [1]. However, beyond scaling advantages, using single molecules in circuits as *sensor elements* enables a broad range of biomolecular sensing applications that integrated circuits cannot otherwise perform. Unlike classical biosensors that rely on indirect reporter methods to detect molecular probe-target interactions (*e.g.,* as in Fig. 12.6.1 with optical, enzymatic, or magnetic reporters), in the molecular electronics approach, current directly passes through a probe molecule, whose interactions with a target molecule are detected through modulation of the probe molecule's conductance [2]. This approach enables label-free, ultra-sensitive, real-time, all-electronic single-molecule sensors to be deployed on low-cost, highly scalable CMOS sensor array chips. The resulting platform extends these "on-chip" advantages to a wide variety of biosensing applications, such as in diagnostics, drug discovery, DNA sequencing, and proteomics [3]–[5].

This work reports the first such CMOS molecular electronic chip for biosensing. As shown in Fig. 12.6.1, the primary molecular sensor element is a ~100GΩ, 25nm long molecular wire composed of an alpha-helical peptide connected to metal nanoelectrodes and a current monitoring circuit. The peptide contains a central conjugation site for attachment of various probe molecules, such as DNA, proteins, enzymes, or antibodies, and is flanked with metal-binding domains for selective coupling to the electrodes. These current monitoring pixels are arrayed with a 20µm pitch into a 16k sensor array on a CMOS device that provides for control of the array and digital data readout at a 1kHz frame rate. The molecular elements are actively "loaded into the circuit" at startup using dielectrophoresis to trap molecules in the nanoelectrodes. Then the current through the bridge molecule under a dc applied voltage is monitored with millisecond temporal resolution. The detected signals are ms-scale current pulses generated by each transient probe-target molecular interaction. This provides direct, comprehensive observation of the single-molecule kinetics, unlike most biosensors that measure ensemble averages of such events.

As shown in Fig. 12.6.2, this chip is arranged like a CMOS image sensor with a 2D pixel matrix divided into 4 sub-arrays, each containing 4,096 (64×64) pixels. A shift-register-based row decoder supplies the control signals (*e.g.*, reset, calibration, etc.) and selects a row of sensors to be read out by column-parallel ADCs butterflied along the array top and bottom. The 64kSps, 8b/10b ADCs are implemented using a single-slope architecture with two preamplifiers and a shared ramp generator (one per side of each sub-array) pitch-matched to the pixel. The ADC outputs are aggregated by a serializer running at 11Mbps with 16 lanes and captured using an off-chip FPGA. The core of the pixel is a capacitive transimpedance amplifier that integrates the pA-level sensor current. The amplifier is implemented with a single-ended, cascoded amplifier (A_v=70dB, *UGBW*=7MHz, I_D=1µA) within the 400µm^2 area constraint. The amplifier bias generation is shared by all pixels in a row. The pixel operation is as follows: 1) During reset (*RST*), the virtual ground node is charged to V_D through a low-leakage switch (guarded by V_D). A bias voltage, V_S, is constantly applied to the other side of the sensor. The amplifier is auto-zeroed at this time to remove its offset and 1/*f* noise. 2) During the integration phase, the sensor current is integrated on a 1b selectable feedback capacitor, C_F=200fF (150pA dynamic range) or 400fF (300pA dynamic range). Normal operation ping-pongs between reset (15.625µs) and integration (984.375µs) in a rolling shutter mode. At startup, a switch (*MODE*) removes the sensor from the circuit, and a calibration current is applied to measure the gain, which is subsequently digitally corrected. The amplifier drives a split buffer, half of which is inside the pixel, with the rest shared by all pixels in the column. This architecture has higher linearity than a conventional source follower-based column bus driver since it is inherently a current-mode circuit with low impedance nodes for fast settling when switching rows.

The precision-engineered molecular wires of interest, such as double-stranded DNA or helical peptides [6], are by design at the nm scale (<30nm), thus requiring the gap between the electrodes to be smaller than possible in CMOS back-end-of-the-line metallization. Also, the electrodes must be electrochemically stable in ionic solutions, precluding standard metals like copper and aluminum. As shown in Fig. 12.6.3, ruthenium metal nanoelectrodes were fabricated using electron-beam (E-beam) lithography or conventional photolithography. For E-beam electrodes, vias to the top metal are exposed by etching away a sacrificial 23µm×15µm "bond pad" to expose a common staging area for the electrodes of 4 adjacent pixels. The 50nm wide electrodes are patterned, then fabricated using a sputtering and liftoff process. A second sputtering step caps the vias and covers part of the wire with oxide to minimize current leakage into the electrolyte. For conventional photolithography, the wafers are pulled before passivation with individual top metal pads exposed for each electrode. Vias and passivation are subsequently added. The nanoelectrodes are patterned with 193nm immersion lithography, and gap narrowing techniques reduce the gap from ~150nm to ~20nm. The electrodes are passivated with a 100nm oxide to minimize the leakage current.

This chip was fabricated in a 180nm CMOS process and operates off a 2.1V supply for the pixels and buffer and 1.8V for the remaining circuits, consuming 58mW (37.8mW for pixels and buffers, 6.3mW for bandgap and bias generation, and 14.4mW for the ADCs and digital). Wafers were post-processed to fabricate nanoelectrodes with a range of gaps (10-12nm, 14-16nm, 17-20nm, and 20-30nm). Chips were wire-bonded with partial encapsulation to expose the pixel array and mounted in a custom flow cell with a rooftop pseudo-reference electrode. The measured input-referred noise is 39fA$_{rms}$ (C_F=200fF) and 76fA$_{rms}$ (C_F=400fF). Figure 12.6.4 shows the measured signal path (pixel and ADC) linearity acquired by sweeping the calibration current. The average differential non-linearity (DNL) is +1.5/-0.7 LSB, and the integrated non-linearity (INL) is ±2 LSB. The residual offset is 2.5-to-5pA across the array due to the buffer and ADC preamplifier offsets, which are not auto-zeroed. Without a bridge, the measured leakage current fluctuates by <1pA dry and 3pA wet in distilled water, with minimal dependence on V_{DS} (nominally V_D=1.3V and V_S=0.8V).

For use, the bridge molecules must be loaded into the circuit. Passive diffusion would take over 24 hours, even at a high concentration. Instead, active dielectrophoretic trapping is employed by applying an ac voltage to the electrodes for a 10-second interval, as shown in Fig. 12.6.5. The "boot up" phase consists of up to 10 rounds of active bridging, applying a 1.6V$_{pp}$ sinusoid at 100kHz through V_S with V_D held at a fixed potential. A low ionic strength solution prevents debye screening. After each round, the array is read to determine if a bridge was incorporated, as observed by an increase in pixel current. A pixel is marked as bridged if two successive measurements show an elevated current, and trapping is stopped to prevent additional bridging. An exemplar SEM image of a single "dumbbell" bridge (two 10nm diameter gold beads capping a 25nm dsDNA molecular wire) spanning the electrode gap is shown for molecular visualization.

To demonstrate the versatility of this platform, we show three different biosensing schemes in Fig. 12.6.6. First, a 17-mer ssDNA probe was attached to the peptide bridge. In the presence of the complementary oligo, the bridge current exhibits pulses corresponding to individual binding/release events. As expected, the pulse widths remained nearly constant, but the pulse rate increased with the target molecule concentration. Next, a DNA aptamer against the spike (S) protein of SARS-CoV-2 was conjugated to the peptide bridge. In the presence of the S protein, pulses representing individual binding/release events are seen, and the pulse rate increases with protein concentration. Finally, a Phi29 DNA polymerase was coupled to the peptide bridge. With a primed ssDNA template and free nucleotides, the enzyme copying activity was observed in real-time, as pulses representing incorporation events. Such signals could be used for single-molecule DNA sequencing if it is possible to accurately differentiate between pulses for A, G, T, and C events. Critically, for all of the above experiments, the sensor output remained flat in the absence of the target molecule and in the presence of off-target molecules, indicating that the sensor is highly specific, despite being extremely sensitive. This chip can also be used to monitor single-molecule binding interactions for antibody-antigens, drug-receptors, or for monitoring CRISPR/Cas enzyme activity, for example. For such diverse biosensing applications, this platform provides the foundation for creating assays with high levels of multiplexing, rapid response on the scale of seconds, a limit-of-detection down to single-molecules, and a dynamic range of pulse rate spanning many orders of magnitude. In summary, this work presents the first molecular electronics CMOS biosensor and demonstrates its broad utility for single-molecule sensing applications.

References:

[1] A. Aviram et al., "Molecular rectifiers," *Chemical Phys Letters,* 1974.
[2] M. Reed et al., "Conductance of a molecular junction," *Science*, 1997.
[3] N. Xin et al., "Concepts in the design and engineering of single-molecule electronic devices," *Nature Reviews Physics*, 2019.
[4] T.J. Olsen et al., "Electronic measurements of single-molecule processing by DNA polymerase I (Klenow fragment)," *JACS*, 2013.
[5] N.L. Ing et al., "Going the distance: long-range conductivity in protein and peptide bioelectronic materials," *Journal of Phys. Chem. B*, 2018.
[6] J. Bustillo, "Development of the Ion Torrent CMOS chip for DNA sequencing," *IEDM*, 2013.

 978-1-6654-2800-2/22/$31.00

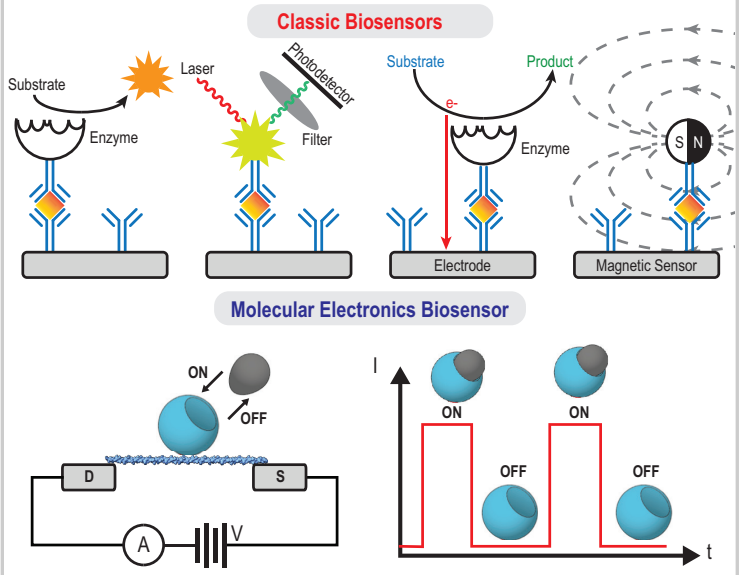

Figure 12.6.1: Overview of classical biosensors and the proposed molecular electronic single-molecule biosensor.

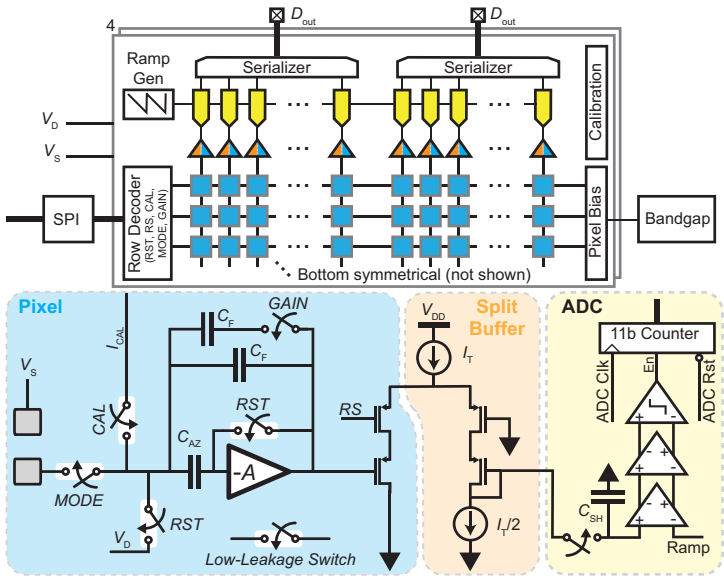

Figure 12.6.2: CMOS sensor array chip architecture (top) and signal path (bottom).

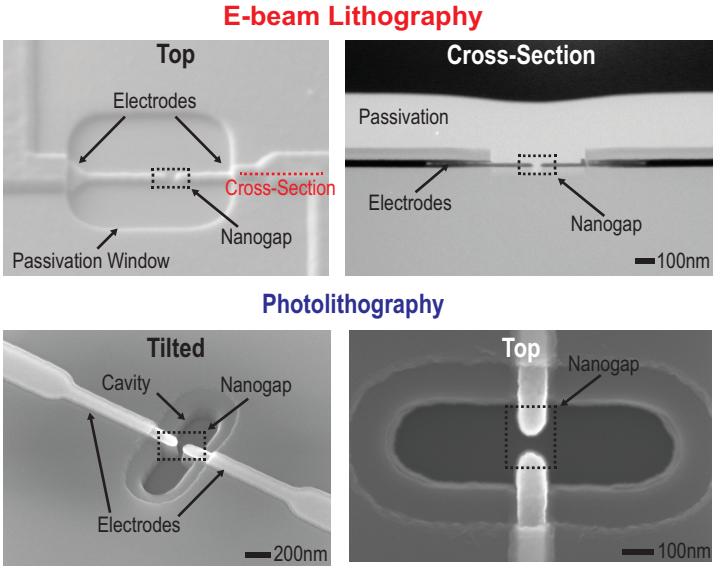

Figure 12.6.3: Scanning electron microscope images of sensor nanoelectrodes fabricated by E-beam and photolithography.

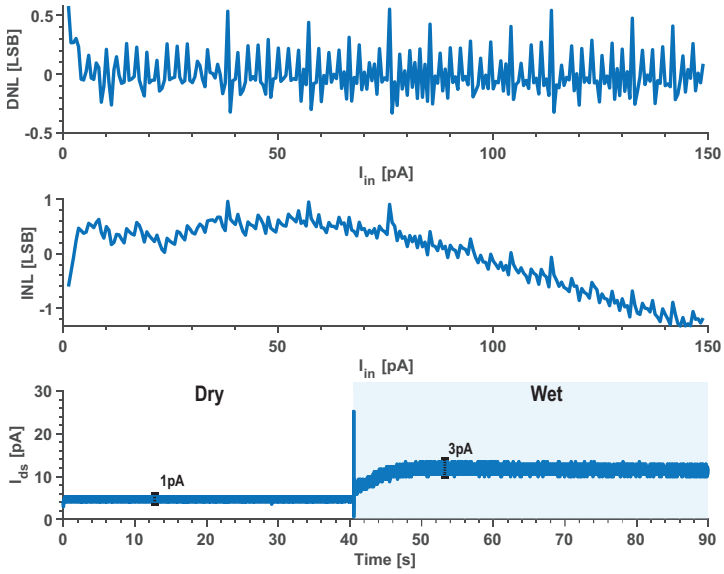

Figure 12.6.4: Electrical measurement results showing linearity of the signal path and dry/wet leakage current signal traces (no bridge).

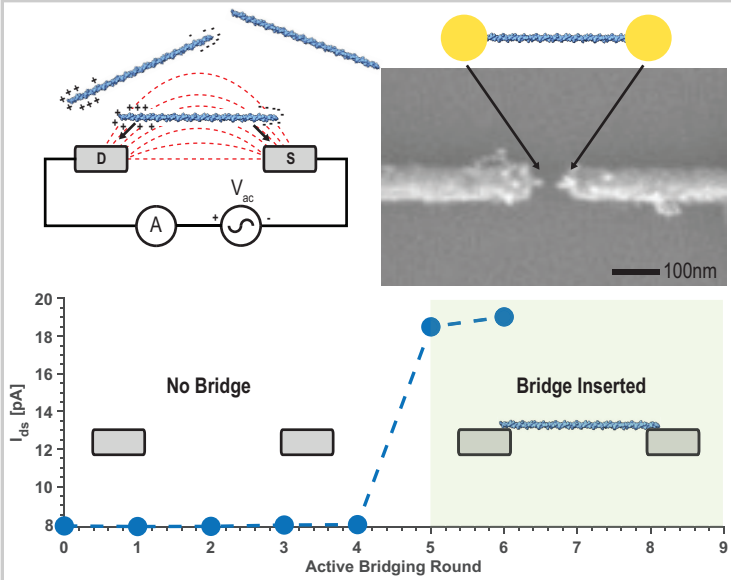

Figure 12.6.5: Dielectrophoretic trapping concept and measured current after successive active bridging rounds, resulting in bridging.

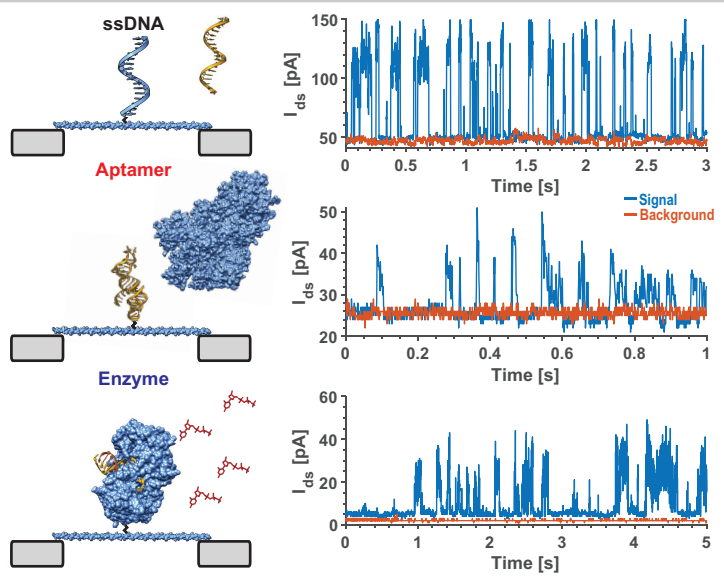

Figure 12.6.6: Molecular electronic sensors and measurement signal trace results (pre-measurement baseline overlay in orange).

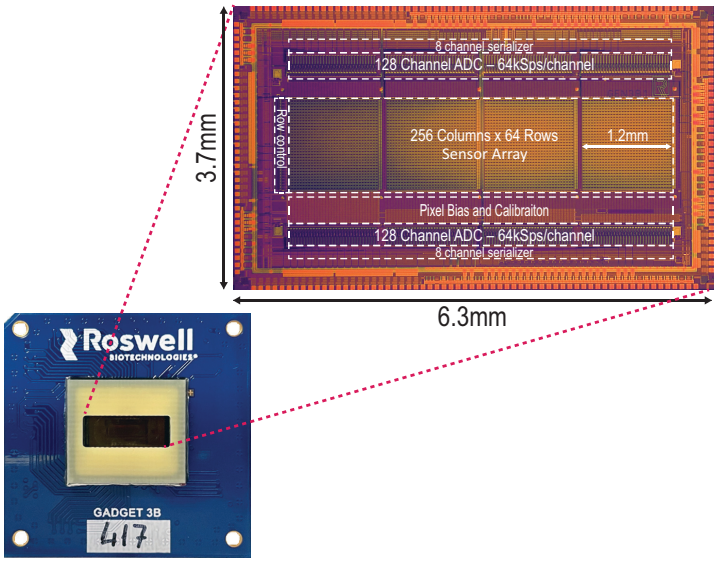

Figure 12.6.7: Annotated die micrograph and fully packaged chip.

978-1-6654-2800-2/22/$31.00